European Journal of Inorganic Chemistry

EurJIC
European Journal of Inorganic Chemistry

Chemistry Europe
European Chemical Societies Publishing

RESEARCH ARTICLE OPEN ACCESS

Ceria Nanostructures Obtained by Hydrothermal Synthesis: Exploring the Experimental Parameter Landscape for Precise Morphology and Size Control

Omar Bettini[1,2,3] | Nicola Da Roit[3] | Andrea De Giacinto[4] | Paolo Dolcet[1,4] | Giulia Bragaggia[1,2] | Jan-Dierk Grunwaldt[3,4] | Silke Behrens[3] | Silvia Gross[1,2,4]

[1]Dipartimento di Scienze Chimiche, Università degli Studi di Padova, Padova, Italy | [2]INSTM, UdR di Padova, Padova, Italy | [3]Institute of Catalysis Research and Technology (IKFT), Karlsruhe Institute of Technology, Eggenstein-Leopoldshafen, Germany | [4]Institute for Chemical Technology and Polymer Chemistry (ITCP), Karlsruhe Institute of Technology (KIT), Karlsruhe, Germany

Correspondence: Silke Behrens (silke.behrens@kit.edu) | Silvia Gross (silvia.gross@unipd.it)

Received: 23 April 2026 | **Revised:** 6 July 2026 | **Accepted:** 9 July 2026

Keywords: filling ratio | hydrothermal synthesis | materials science | microwave synthesis | nanocube | nanomaterials | nanorod | nanostructure size control | specific surface area

ABSTRACT

Many oxidation catalysts rely on ceria nanomaterials as efficient supports for platinum group metal nanoparticles, where morphology affects the catalytic performance. Rational exploitation of the chemical parameter space enables the tuning and control of these morphological features. This study presents a systematic investigation of conventional and microwave-assisted hydrothermal syntheses of ceria nanorods and nanocubes. The specific role of Ce(III) counter-ions in nanorod formation was systematically investigated, identifying chloride ions as essential for anisotropic growth. Microwave heating proved superior to conventional methods, yielding high-aspect-ratio rods in 10 min while preventing the surface area loss associated with thermal coarsening. For the nanocubes, an acid-buffered route was developed to narrow the polydispersity. The reactor filling ratio in the microwave syntheses emerged as a key parameter to modulate solvent evaporation, allowing tuning of the nanocube size (from 14 to 26 nm) and truncation degree. Structural and morphological characterisation by X-ray diffraction (XRD), transmission electron microscopy (TEM) and Brunauer–Emmett–Teller specific surface area analysis (BET) confirmed the formation of highly crystalline and porous nanomaterials, providing a rational framework for the synthesis of ceria nanostructures with controlled morphology via microwave-assisted heating. The effect of autogenous pressure was rationalised by numerical calculations using a Python script developed by the authors.

1 | Introduction

Heterogeneous catalysts based on metal oxides as supports and platinum group metals (PGMs) as active sites are essential for efficient environmental, electrocatalytic and energy-related applications [1]. Beyond the size and shape of the noble metal species, the specific surface area (SSA) and exposed facets of the oxide support, the strength of metal–support interactions [2, 3], as well as the thermal and chemical stability, all play critical roles in determining the catalytic performance and stability under operative conditions. Among the most widely studied oxide supports, particularly interesting for its inherent properties is cerium dioxide (CeO_2), which attracts significant interest due to Ce's natural abundance [4, 5], the possibility of tuning its reducibility through morphological control [6, 7] and its enhanced oxygen storage properties, making it a convenient support for noble metal nanoparticles [5, 8, 9]. The ability of CeO_2 to reversibly exchange oxygen with the environment, commonly referred to as oxygen

storage capacity (OSC), strongly depends on the energy required to generate an oxygen vacancy [6, 8, 10, 11]. For CeO_2, this energy has been shown to be up to 30% lower on the surface than in the bulk [5, 12, 13], highlighting the importance of maximising SSA through nanostructuring. Moreover, ceria can facilitate catalytic reactions, like CO oxidation, either through a Langmuir–Hinshelwood-like mechanism, where both reactants are adsorbed and react on the surface of the active site (oxygen spillover), or, more prominently, through a Mars–van Krevelen-type mechanism [14, 15], in which the lattice oxygen from ceria or the interface takes part in the catalytic cycle without altering ceria's fluorite crystal structure [16]. The oxygen storage and catalytic properties of ceria are also facet-dependent and therefore closely related to nanoparticle morphology [5, 8, 17]. From a thermodynamic standpoint, the stability of CeO_2 surfaces decreases in the order (111) > (110) > (100) [5]. Nanocubes primarily expose six (100) facets, with (110) and (111) surfaces appearing at the corners and edges [18–20]. In contrast, nanorods typically expose (110) and (100) facets, though (111) facets have also been observed [21–25]. Thus, controlling the exposed facets through shape-directed synthesis, together with achieving a homogeneous nanoparticle size distribution, provides a means to tune oxygen vacancy formation and catalytic activity while ensuring consistent properties across the support. Commercially available ceria powders, on the other hand, generally lack preferential facet orientation. In this context, the present study focuses on the shape-controlled synthesis of ceria nanoparticles with cubic and rod-like morphologies. Hydrothermal synthesis [26] was selected as the main approach due to its simplicity [27, 28], its effectiveness in producing materials with uniform properties and narrow size distributions [6] and its well-established ability to direct morphological evolution. In a typical process, the reaction mixture is heated in a sealed vessel above the boiling point of water (>100 °C), developing an autogenous pressure (>1 atm) [29, 30]. To further enhance the process efficiency, microwave-assisted heating was also explored. This technique has been successfully applied to a wide range of inorganic and organic syntheses [31, 32] and offers several advantages: it markedly shortens reaction times [33–36], improves energy efficiency by directly heating the solvent [33, 37] and minimises thermal gradients within the reaction medium. Microwave heating operates through ionic conduction and dipolar polarisation [31, 38], where heat is generated by the oscillatory motion of ions and dipoles in the electromagnetic field. Reaction time is essential for controlling particle size, and the choice of mineraliser strongly influences the growth mechanism [39–42]. For instance, chloride ions are known to favour the formation of nanorods, whereas nitrate ions promote nanocube growth [6, 43]. Additionally, nitrate ions have been reported to facilitate the oxidation of $Ce(OH)_3$ to CeO_2 under alkaline conditions [6, 43]. Although hydrothermal routes for producing ceria nanorods and nanocubes are well established, current literature presents several limitations that restrict reproducibility and morphological control. Most syntheses rely on strongly alkaline environments and typically produce nanocubes with broad size distributions and characteristic lengths often exceeding 100 nm [43, 44]. Acid-mediated routes remain comparatively less explored, even though the presence of acetate ions has been reported to stabilise specific growth directions and potentially narrow the particle size distribution [45]. Furthermore, the influence of key experimental parameters, such as filling ratio, precursor counter-ions and solvent dielectric properties, is often discussed qualitatively but rarely investigated systematically, leaving open questions regarding their individual contributions to nucleation and growth. To address these gaps, the present study systematically examines how selected hydrothermal synthesis parameters affect the morphology of ceria nanoparticles. For nanorods, the role of different Ce(III) salts was evaluated together with the impact of the filling ratio on nucleation-growth dynamics and the potential of microwave heating to shorten reaction times without compromising product quality. For nanocubes, an acid-buffered synthesis inspired by Lyu et al. [46] was adapted and optimised, demonstrating that acetate-mediated growth under acidic conditions can yield highly uniform nanocubes with mean sizes around 20 nm, substantially smaller and less polydisperse than those typically obtained by conventional alkaline syntheses. In addition, the effects of reaction time, filling ratio and the addition of ethanol, used to modulate the dielectric constant of the medium, were systematically investigated for both heating modes, providing a comprehensive understanding of how each parameter shapes the final particle morphology.

2 | Experimental Methods

2.1 | Materials

Cerium (III) acetate hydrate (Sigma–Aldrich, 99.9% trace metals basis), cerium (III) chloride heptahydrate (Sigma–Aldrich, 99.9% trace metals basis; Fisher Scientific, 99%), cerium (III) nitrate hexahydrate (Sigma–Aldrich, 99.9% trace metals basis; Fisher Scientific, 99%), sodium hydroxide (Sigma–Aldrich, ACS reagent, 97%, Acros Organics), acetic acid (HAc, Sigma–Aldrich/Acros Organics, glacial), ethanol (Fluka, 96%; Sigma–Aldrich, 99.65%), sodium acetate (NaOAc, Carlo Erba, Merck, 99%)

2.2 | Sample Labelling

Sample labels follow this nomenclature: NR_MW_43%_1h refers to nanorods (NR) obtained via microwave-assisted (MW) synthesis, with a 43% v/v filling ratio and a 1 h reaction time. NC_C_46%_E4_24h_L refers to conventionally (C) synthesised nanocubes (NC), with a 46% filling ratio, an ethanol–water volume ratio of 1:4 (E4), a reaction time of 24 h, and a low precursor concentration (indicated by L). If a high precursor concentration was used, the L suffix is omitted.

2.3 | Conventional Hydrothermal Synthesis of Nanorods

For the conventional hydrothermal synthesis (a summary of chloride-based syntheses is reported in Table S1), the CeO_2 nanorods were prepared in two different reactors, maintaining a constant 43% vol/vol filling ratio throughout. In the 23 mL reactor (Parr steel reactor, 4745 general purpose acid digestion bomb - Parr Instrument Company), 1 mL (1 mmol) of a 1 M aqueous solution of $CeCl_3{\cdot}7H_2O$, $Ce(NO_3)_3{\cdot}6H_2O$ or $Ce(OAc)_3{\cdot}xH_2O$ was added dropwise to 9 mL (90 mmol) of 10 M NaOH. After stirring for 20 min, the mixture was sealed and placed in an oven preheated to 100 °C for 6 or 24 h. The ceria nanoparticles were

collected by centrifugation at 11 267 rcf (Relative Centrifugal Force) for 5 min, utilising a Z32-HK centrifuge (Hermle). The precipitate was washed twice with 15 mL of deionised water. Centrifugation was performed at each step to recover the precipitate. Subsequently, the precipitate was washed using 5 mL of ethanol and then dried overnight at 80 °C in air. In the 210 mL reactor, the volume of the solution was increased by a factor of 9.1, reaching a final volume of 91 mL, for reaction times of 0.5, 1, or 6 h. All other parameters were kept the same.

2.4 | Conventional Hydrothermal Synthesis of Nanocubes

A modified procedure originally reported by Lyu et al. [46] was used for the synthesis of nanocubes in acidic media. Starting with the conventionally heated synthesis (summary reported in Table S2), 1.5 mmol of $Ce(NO_3)_3{\cdot}6H_2O$ was dissolved in 20 mL of a mixture of ethanol (2.5 mL) and deionised water (17.5 mL) at a 1:7 vol/vol ratio in a 50 mL Teflon liner. After stirring for 15 min, 36.6 mmol of NaOAc and 53 mmol of HAc were added, reaching a final filling ratio of 46% vol/vol. The slurry, sealed in a stainless-steel Parr reactor, was then kept in a preheated oven for 24 h at 200 °C. Once cooled to room temperature (RT), the suspension was centrifuged at 13 250 rcf for 7 min. The precipitate was then washed three times with 10 mL of EtOH and left to dry overnight. The synthesis was scaled up in the 210 mL Teflon liner by increasing the amount of the reactants by a factor of 4.2. The effects of the reaction environment were investigated by changing the solvent and cerium precursor concentrations and increasing the ethanol–water volume ratio from 1:7 to 1:4 as well as the amount of cerium nitrate by a factor of 2.85 (using a total of 18 mmol). Reaction times of 4, 12, 18 and 24 h were tested under these reaction conditions.

2.5 | Microwave-Assisted Hydrothermal Synthesis of Nanorods

In the microwave-assisted synthesis of nanorods (summary reported in Table S3), a 100 mL Teflon liner (XP-1500 plus vessel, CEM) was utilised, with filling ratios of 11%, 22% and 43% by volume. For the lowest ratio (11%), 1.13 mL of the cerium chloride solution was added to 10.23 mL of 10 M NaOH, doubling and quadrupling these volumes to achieve the other two filling ratios (22% and 43%, respectively). The same mixing steps described above were followed, and the reactor was then heated in a microwave oven (CEM Corporation MARS 5 Digestion Microwave System) to 100 °C at a power of 400 W and a heating ramp of 3 min. The temperature was maintained at 100 °C for either 10 min or 1 h. The centrifugation and drying steps were carried out as described in Section 2.3.

2.6 | Microwave-Assisted Hydrothermal Synthesis of Nanocubes Under Acidic Conditions

A 100 mL Teflon liner was used for the microwave-assisted hydrothermal synthesis of nanocubes (summary in Table S4). In this setup, the amounts of reactant and solvent used in the reaction (which used 18 mmol of cerium nitrate and an ethanol–water ratio of 1:4) were halved, keeping a 46% vol/vol filling ratio. After 15 min of stirring, the reactor was sealed, placed in a microwave oven, and heated to 200 °C at 400 W with a ramp of 10 min. It was then maintained at 200 °C for 4 h. After cooling to RT, the particles were collected by centrifugation at 7197 rcf, washed three times with 15 mL aliquots of acetone and dried in an oven at 80 °C overnight. With the microwave-assisted approach, the effect of the filling ratio was investigated by performing syntheses at 11%, 23% and 46% vol/vol, using only water as the solvent and changing the amount of the other reactants accordingly.

2.7 | Characterisation Methods

2.7.1 | *X-ray Diffraction (XRD)*

The crystalline structure and phase purity of the nanoparticle powders were determined by XRD analysis. XRD patterns were recorded using a PANalytical X'Pert Pro X-ray diffractometer employing a 2θ Bragg–Brentano geometry with Cu-K_α radiation ($\lambda = 1.5406$ Å) and a Ni filter. Bragg angles ranging from 20° to 80° (2θ) were recorded over a period of 12 min at RT with a step size of 0.3°. The reflections were analysed by X'Pert Highscore Plus (PANalytical) and compared with reference data reported in the International Centre for Diffraction Data (ICDD) database, JCPDS 34-0394.

2.7.2 | *Transmission Electron Microscopy (TEM) and Size Distribution*

The size, size distribution and morphology of the ceria nanoparticles were analysed on an FEI Tecnai G2 TEM, operating at 100 kV, equipped with an Olympus Veleta camera and a TVIPS F114 camera. The particle sizes were manually measured using ImageJ, and the data are presented as median ± median absolute deviation. The corresponding length distribution histograms and particle counts for each sample are provided in the Supporting Information (Figures S1–S5), along with a summary of the total particles counted (Table S5). Additional TEM images are also available in the SI (Figures S6–S31).

2.7.3 | *Measurement of the SSA*

The SSA was determined by N_2 physisorption. The measurements were taken on a NOVA2200e (Quantachrome Instruments) with N_2 at 77 K in a relative pressure range between 0.005 and 1 p/p_0. Prior to measurement, the samples were degassed at 200 °C for 20 h at 1 Torr (0.0013 bar). The data were evaluated with the NOVA Win Software (Version 11.03). The SSA was determined using the Brunauer–Emmett–Teller (BET) [47] model (DIN ISO 9277:2010), accounting for the Rouquerol criteria.

2.8 | Repetition of the Experiments

To ensure that the reported morphological data and size distributions are representative of the synthetic protocol rather than an isolated event, products from at least three independent batches for each formulation were pooled prior to characterisation.

3 | Results

3.1 | CeO_2 Nanorods

As reported by Trovarelli and Llorca [6], the role of the Ce(III) precursor counter-ions is crucial in defining the final morphology of the nanoparticles, because their selective adsorption on specific crystal planes modifies the surface free energy, thereby altering the relative growth kinetics of those facets. For example, chloride ions are known to stabilise the (111) facets, which promotes anisotropic growth into one-dimensional (1D) structures such as nanowires and nanorods, while nitrate ions stabilise the (100) facets, favouring the development of nanocubes. This ion–specific interaction acts as an intrinsic structure-directing effect, even in the absence of external surfactants or templates. Accordingly, a systematic study of the hydrothermal synthesis of ceria nanorods was conducted by varying the Ce precursor and the reaction time. The experiments were performed by adopting the strongly basic method (9 M NaOH) originally reported by Mai et al. [48]. The chosen precursors were: $Ce(OAc)_3{\cdot}xH_2O$, $CeCl_3{\cdot}7H_2O$ and $Ce(NO_3)_3{\cdot}6H_2O$ (reactor volume 23 mL). Furthermore, the influence of reaction time was investigated by conducting experiments at 6 and 24 h. For all syntheses, the yield exceeded 70% of the theoretical value, with the nitrate precursor giving the highest molar yields, and the acetate precursor the lowest. Phase purity of the products obtained with the three different precursors was confirmed by XRD analysis (Figure 1) for all reaction times (6 and 24 h).

The XRD patterns of all samples (Figure 1) revealed the characteristic reflections of the CeO_2 phase with a fluorite-type structure (JCPDS 34-0394), corresponding to diffraction peaks at 2θ angles of 28.5°, 33.0°, 47.4°, 56.3°, 59.1°, 69.6°, 76.7° and 79.1°. The broad reflections observed in the XRD patterns indicate small crystallite sizes. Analysis using the Scherrer equation confirms a consistent increase in crystallite size with longer reaction times [49] (see Table 1). Notably, nanorods synthesised from chloride and nitrate precursors exhibited larger crystallite sizes than those obtained with acetate. This is attributed to the strong capping effect of acetate species, which, as reported by Fu et al. [45], significantly retards crystal growth kinetics.

TEM analysis revealed that all synthesised products share a common intertwined morphology with a marked tendency towards agglomeration, the extent of which increased with reaction time. However, distinct morphological evolution was observed, depending on the precursor. When cerium acetate was used, the resulting nanoparticles were the least morphologically uniform. Determination of the aspect ratio (width/length) for the 6 h sample was prevented by the extensive overlap of nanorod edges (Figure 2a), while nanocubes were clearly visible alongside rods in the 24 h sample (Figure 2b). Conversely, the chloride precursor facilitated the complete formation of nanorods within 6 h. Although some small, undefined particles persisted, these nanorods maintained a stable aspect ratio of approximately 0.14 across the 6 h (Figure 2c) and 24 h marks (Figure 2d), indicating well-preserved anisotropic growth. The nitrate precursor (Figure 2e,f) exhibited a high degree of agglomeration. These results confirm the significant impact of counter-ions on morphology [6], underlining the importance of precursor choice. In agreement with previous reports by Fu et al. [45] and Wu et al. [43], the acetate precursor appeared to be the least suitable for nanorod synthesis, likely due to the capping behaviour of acetate ions, which hinders anisotropic growth and favours the formation of more isotropic or faceted morphologies [45].

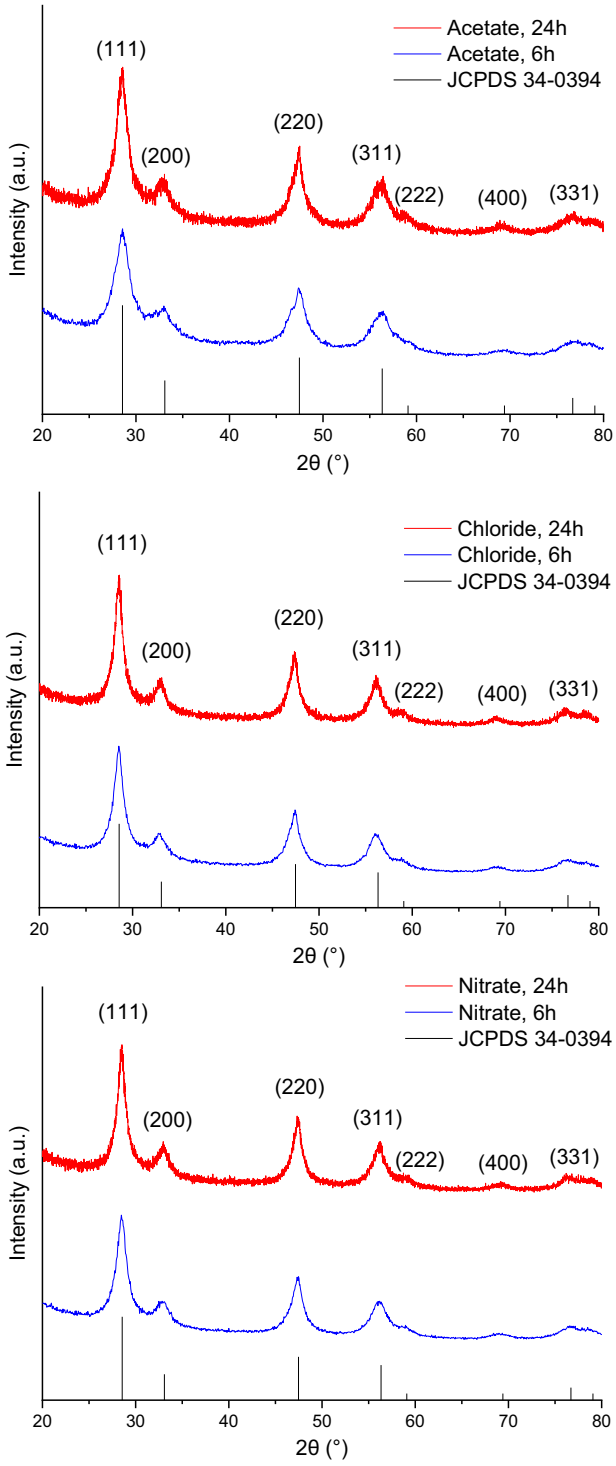

FIGURE 1 | XRD patterns of ceria nanorods obtained from different Ce precursors at different reaction times with the conventional synthesis.

Based on the screening results, $CeCl_3{\cdot}7H_2O$ was selected as the optimal precursor for the subsequent experiments. This decision is further supported by literature observations [6], which suggest that nitrate ions facilitate the premature oxidation of dissolved

TABLE 1 | Crystallite size of ceria nanorods, calculated by applying the Scherrer equation to the (111), (220) and (331) reflections (averaged value), and aspect ratio for samples obtained from different Ce precursors and after different reaction times.

Ce precursor	Reaction time, h	Average crystallite size, nm	Average aspect ratio, width/length
$Ce(NO_3)_3{\cdot}6H_2O$	6	5.8 ± 0.9	0.13 ± 0.02
	24	6.8 ± 1.0	0.11 ± 0.01
$CeCl_3{\cdot}7H_2O$	6	6.0 ± 1.0	0.14 ± 0.01
	24	7.0 ± 1.1	0.14 ± 0.02
$Ce(OAc)_3{\cdot}xH_2O$	6	4.5 ± 0.8	—
	24	5.2 ± 0.9	0.11 ± 0.02

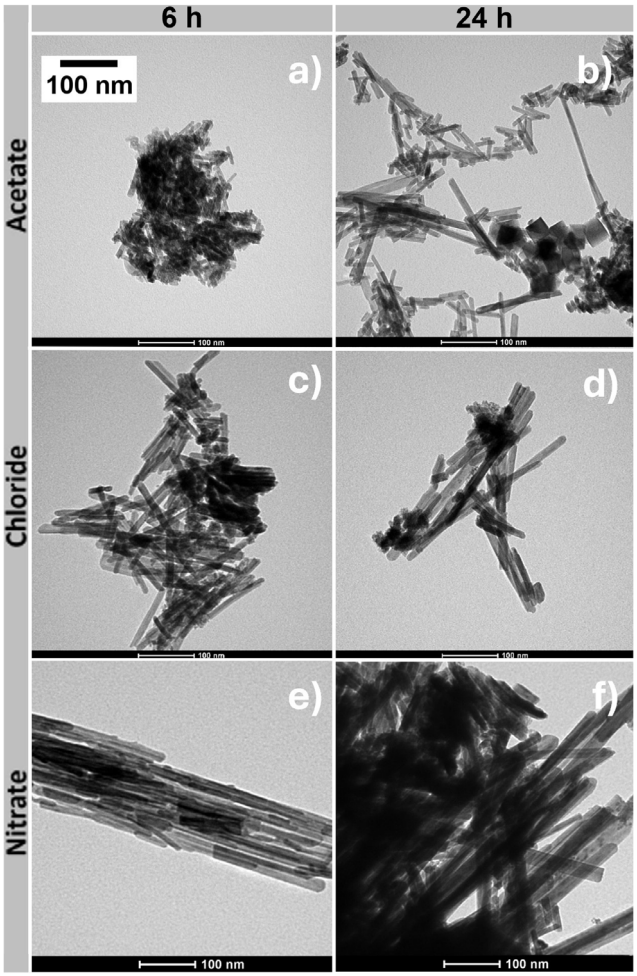

FIGURE 2 | TEM images of nanorods obtained from different precursors: $Ce(OAc)_3{\cdot}xH_2O$ (a,b), $CeCl_3{\cdot}7H_2O$ (c,d) and $Ce(NO_3)_3{\cdot}6H_2O$ (e,f) after 6 h (a,c,e) and 24 h (b,d,f).

$Ce(OH)_3$ intermediates; this rapid oxidation mechanism often leads to poorly defined nanoparticles and disrupts the kinetics required for effective nanorod growth. To evaluate the reproducibility of the protocol at a larger scale, the reaction volume was increased from 23 mL (Figure 3a) to 210 mL (sample NR_C_43%_6 h, Figure 3b). As evidenced by the morphological comparison and the dimensional data in Table 2, this ninefold increase in scale did not negatively impact product quality. The aspect ratio and morphology remained consistent, demonstrating that the synthesis results are not significantly affected by this change in reactor volume and geometry.

To evaluate whether a shorter reaction time could improve size control [50], the reaction duration was reduced by factors of 6 (NR_C_43%_1 h) and 12 (NR_C_43%_30 min) in the 210 mL liner. Well-defined nanorods were successfully obtained in both cases (Figure 3c,d). However, the 30 min sample exhibited a noticeably higher degree of agglomeration compared to the 1 h product. This behaviour is likely due to the incomplete evolution of the intermediate phase at such short times: residual amorphous species may persist at the grain boundaries, acting as binders that promote aggregation during recovery. Extending the time to 1 h seemingly allows for their consumption and surface maturation. Microwave heating is well known for its fast and homogeneous heating; moreover, it was reported by the authors in a complementary article [51] to be more efficient than conventional heating from an environmental point of view. This approach was therefore employed to investigate the impact of short reaction times further and to potentially accelerate nucleation and growth processes. As shown in Figure 4c,d, nanorods were successfully synthesised in 1 h (NR_MW_43%_1 h) or even in as little as 10 min (NR_MW_43%_10 min), respectively, using a 100 mL liner. Moderate agglomeration was still present, similar to the fast conventional runs. The formation of nanorods in this additive-free system is attributed to the pronounced structural anisotropy of the $Ce(OH)_3$ nuclei formed in the strongly alkaline environment (9 M NaOH) [48], which promotes a high dissolution-reprecipitation rate [52]. This intrinsic shape-directing effect is particularly advantageous, as it obviates the need for external directing agents (e.g., oleic acid, PVP), which are often required in other protocols [53]. Finally, varying the filling ratio in the MW setup (11%, 22% and 43%) yielded nanorods with comparable dimensions and reduced agglomeration (Figure 4a–c, respectively; Table 3), confirming the flexibility of the process. At 100 °C, the total pressure inside the vessels reaches approximately 2.3 bar. This pressure is insufficient to generate markedly different reaction conditions, as solvent evaporation remains limited regardless of the filling ratio (Table S6). Consequently, the resulting products exhibit consistent SSA and comparable lengths (Table 3).

Notably, the SSA and particle length obtained by microwave-assisted synthesis were comparable to those of the conventional route, as evidenced by comparing NR_C_43%_6 h with NR_MW_43%_1 h, and NR_C_43%_1 h with NR_MW_43%_10 min (Tables 2 and 3). However, microwave-assisted synthesis required only one-sixth of the reaction time. The evolution of SSA values further highlights these trends. In the conventional process (210 mL liner), the SSA decreased with reaction time from 115 (30 min) to 84 $m^2 g^{-1}$ (6 h). Interestingly, the same 6 h treatment performed in the smaller 23 mL liner retained a significantly higher SSA (108 $m^2 g^{-1}$). This discrepancy suggests that the reactor scale, and the associated thermal gradients, affect the extent of coarsening during prolonged hydrothermal treatment. In contrast, microwave syntheses consistently yielded high SSAs (between 88 and 110 $m^2 g^{-1}$), with the 10 min sample approaching the values of the fastest conventional runs.

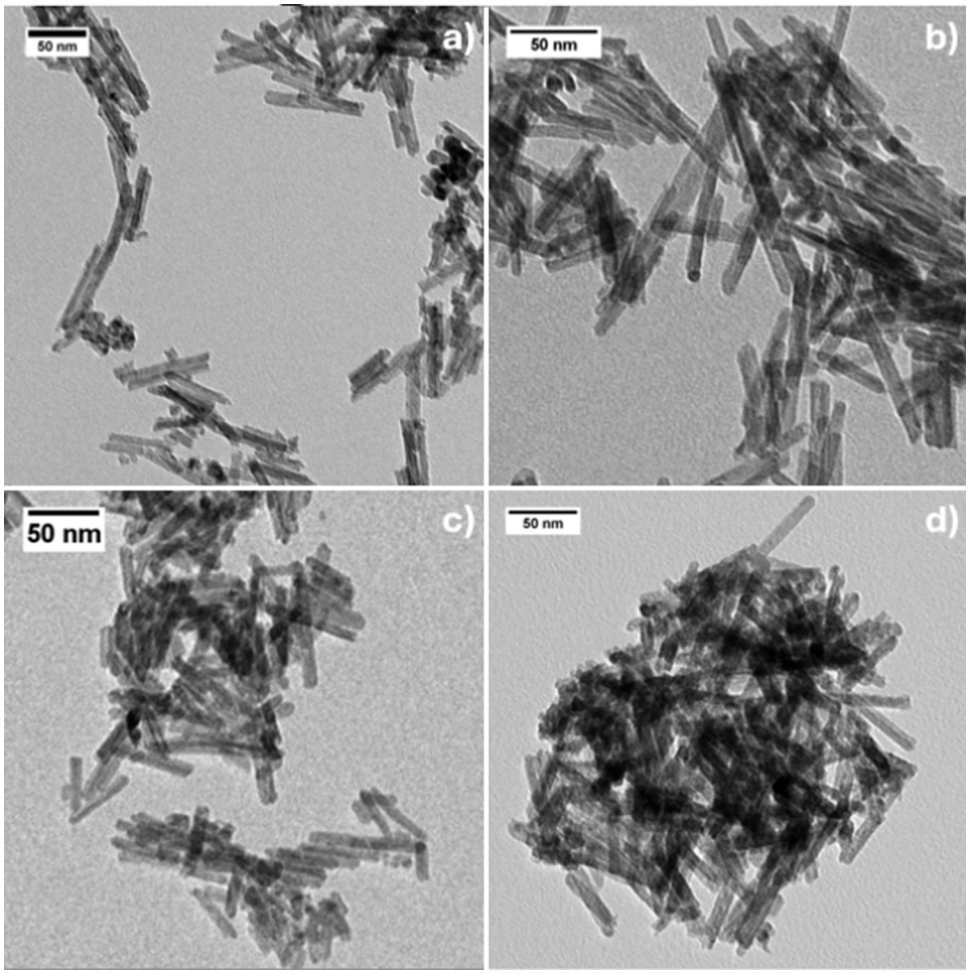

FIGURE 3 | Nanorods synthesised in the 23 mL liner with a reaction time of 6 h (a) or in the 210 mL liner with a reaction time of 6 h (b), 1 h (c) and 30 min (d).

TABLE 2 | Dimensional analysis of the nanorods synthesised in the 23 and 210 mL liner with a reaction time of 6 h.

Sample name	NR_C_43%_30 min	NR_C_43%_1 h	NR_C_43%_6 h	
Liner volume	210 mL			23 mL
Length, nm	—	50 ± 11	51 ± 17	51 ± 18
Aspect ratio, width/length	—	0.16 ± 0.04	0.15 ± 0.05	0.15 ± 0.05
SSA, m^2/g	115	113	84	108

Consequently, microwave processing offers a substantial reduction in reaction time without significant loss in SSA.

3.2 | Nanocubes

Standard literature protocols for obtaining ceria nanocubes typically employ highly concentrated NaOH at elevated temperatures (ca. 180 °C) and long reaction times (over 6 h) without capping agents [6, 19, 52, 54]. However, this approach typically yields large particles (with an edge length of up to 200 nm) with a broad size distribution [52, 54]. To overcome this limitation and achieve smaller and more uniform nanocubes, we adopted a modified procedure using an acetic acid/sodium acetate buffer solution (pH ≈ 4.6), based on the protocol by Lyu et al. [46], which is known to inhibit nanorod formation [45]. A systematic investigation was conducted to assess the impact of solvent composition and reactor scale. Initial syntheses using water as the sole solvent (NC_C_46%_24 h_L) resulted in a negligible yield (5%). This low recovery is likely due to the formation of highly stable colloidal nanoparticle suspensions, which resisted efficient sedimentation during centrifugation.

To address the low yields and stability issues observed in pure water, the solvent composition was modified by introducing ethanol. The addition of ethanol lowers the overall dielectric constant of the mixture (ca. 55 at 20 °C for the ethanol–water 1:4 volume ratio [55], compared to 80 for pure water [56]), thereby

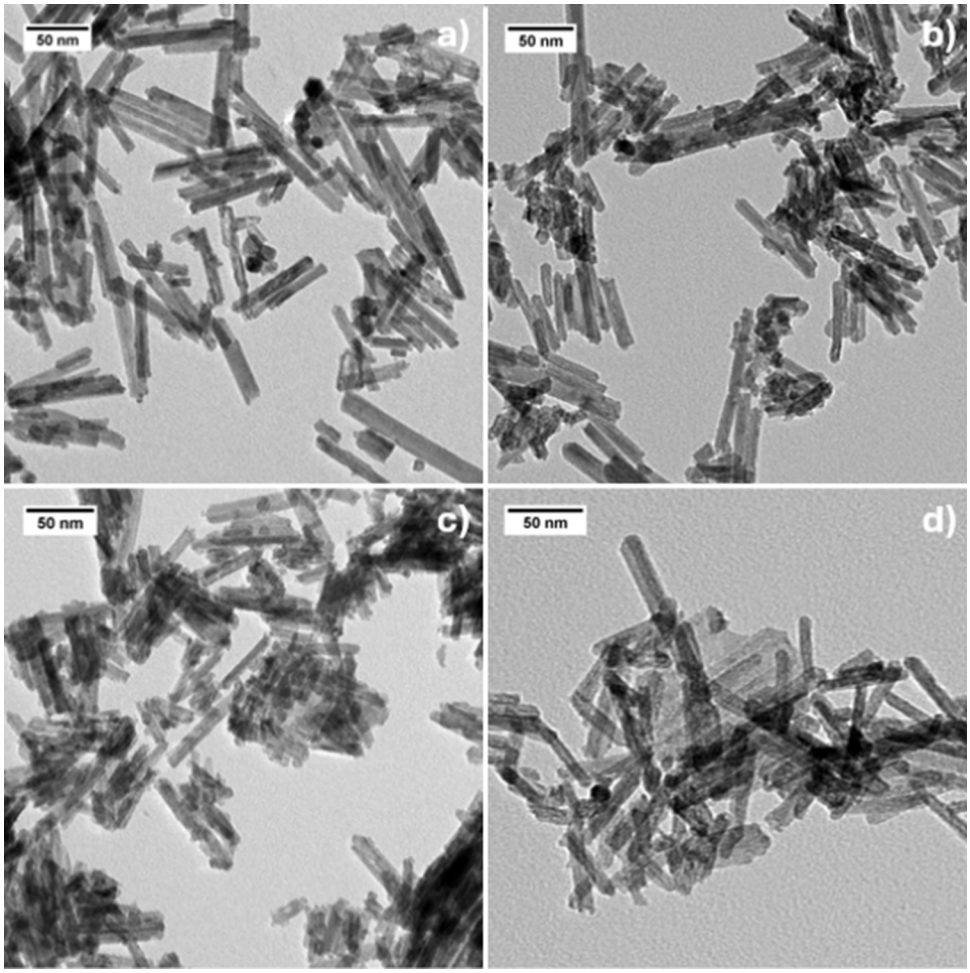

FIGURE 4 | Nanorods synthesised with the microwave-assisted hydrothermal synthesis. Filling ratios of 11% (a), 22% (b) and 43% (c) were investigated. Reaction time: 1 h (a–c), and 10 min (d, filling ratio of 43%).

TABLE 3 | Dimensions of the nanorods synthesised in the microwave oven were calculated by applying the Scherrer equation to the (111), (200), (220) and (311) reflections.

Sample name	NR_MW_11%_1 h	NR_MW_22%_1 h	NR_MW_43%_1 h	NR_MW_43%_10 min
Length, nm	63 ± 21	55 ± 18	46 ± 16	40 ± 15
Aspect ratio, width/length	0.15 ± 0.06	0.16 ± 0.04	0.15 ± 0.03	0.17 ± 0.04
SSA, m^2/g	89	88	88	110
Average crystallite size, nm	7.7 ± 0.4	6.7 ± 0.5	6.4 ± 0.3	—

reducing the precursor solubility and promoting supersaturation (S) even at lower solute concentrations. Consequently, the nucleation rate (J) is enhanced according to the classical nucleation theory: $J_n \propto \exp(-1/(\ln S)^2)$. This exponential increase in nucleation rate leads to a higher number of nanoparticles and improved material recovery; the yield rose to 23% and 30% using ethanol/water vol. ratios of 1:7 and 1:4, respectively. Despite this improvement, TEM analysis (Figure 5a–c) revealed that well-defined nanocubes were still scarce. Moreover, scaling up the reaction to a 210 mL liner (keeping the 1:4 ratio) proved detrimental, reducing the yield to 21% and further decreasing the number of cube-shaped particles (Figure 5c). This suggests that nanocube formation in this buffer system is highly sensitive to reactor geometry and the associated thermal gradients. Recognising that precursor concentration is another critical parameter governing growth [6], the concentration was increased from 0.065 to 0.186 M for the synthesis of sample NC_C_46%_E4_24 h (Figure 6d). This adjustment resulted in a significant improvement in product quality: well-defined nanocubes were obtained with an average edge length of 16 ± 3 nm (Table 4), a narrow size distribution and a markedly increased reaction yield of 55 mol% (Table S8).

To clarify the kinetic evolution of the system, the reaction time was varied to 4, 12 and 18 h (samples NC_C_46%_E4_4 h, _12 h, and _18 h, respectively). Cube-like nanoparticles were already

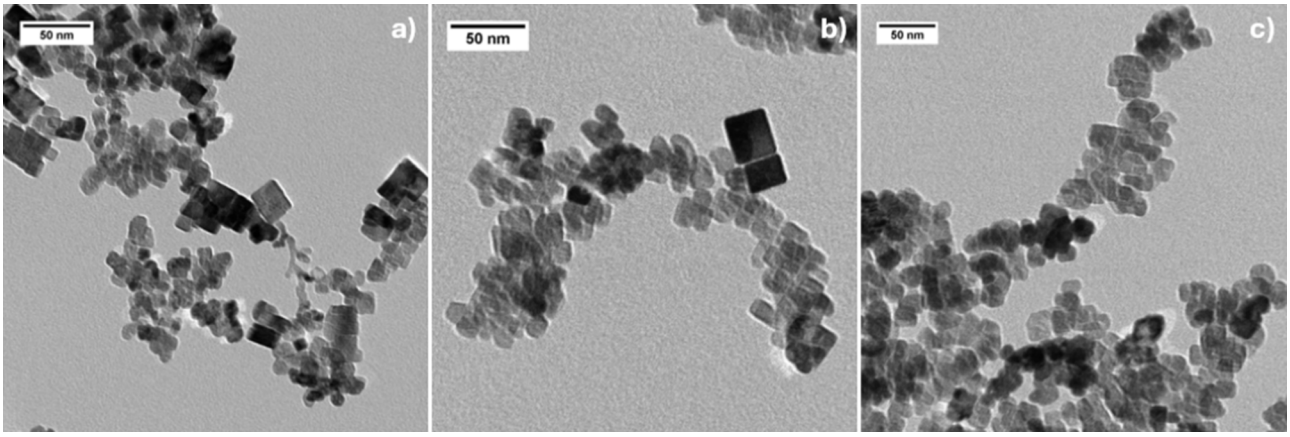

FIGURE 5 | Ceria nanocubes synthesised under acidic conditions, using a 50 mL Teflon liner with ethanol–water volume ratios of 1:7 (a) and 1:4 (b). In (c), the reaction was conducted with the same 1:4 ratio but in a 210 mL Teflon liner.

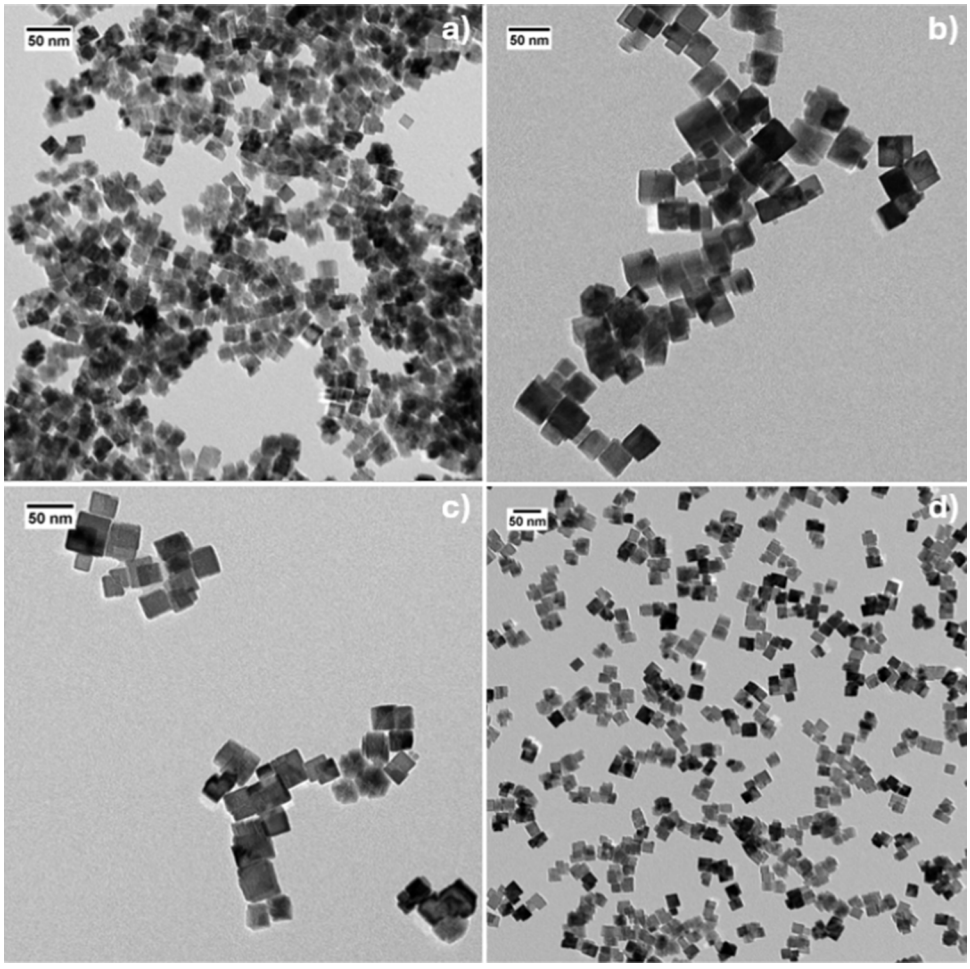

FIGURE 6 | TEM images of the nanocubes obtained by conventional synthesis in the 210 mL Teflon liner with a 46% filling ratio and a reaction time of 4 h (a), 12 h (b), 18 h (c) and 24 h (d).

observed after just 4 h, despite some morphological imperfections (Figure 6a). Extending the thermal treatment to 12 and 18 h significantly improved the shape definition, yielding well-faceted nanocubes (Figure 6b,c, respectively). The reaction yield followed a distinct non-monotonic trend: starting from 12% after 4 h, it increased to 68% after 12 h, reaching 79% after 18 h, before dropping to the previously discussed 55% after 24 h. The low yield after 4 h may be due to incomplete reaction kinetics, where a significant proportion of the precursor remains unreacted, or the nuclei may not have attained the critical radius required for efficient sedimentation during centrifugation. Conversely, the decrease in yield observed at 24 h suggests that the optimal

TABLE 4 | Dimensional analysis of nanocubes synthesised using the conventional approach. Crystallite sizes were calculated using the Scherrer equation for the (111), (200), (220) and (311) reflections.

Sample name	NC_C_46%_24 h_L	NC_C_46%_E7_24 h_L	NC_C_46%_E4_24 h_L (liner 50 mL)	NC_C_46%_E4_4 h_L (liner 210 mL)
Edge length, nm	16 ± 3	17 ± 5	16 ± 3	15 ± 2
Sample name	**NC_C_46%_E4_4 h**	**NC_C_46%_E4_12 h**	**NC_C_46%_E4_18 h**	**NC_C_46% _E4_24 h**
Edge length, nm	14 ± 2	29 ± 4	24 ± 3	16 ± 2
SSA, m^2/g	48	25	24	42
Average crystallite size, nm	14.4 ± 0.1	26.0 ± 0.4	24.5 ± 0.7	17.3 ± 0.1

equilibrium between nucleation and growth is achieved between 12 and 18 h. Beyond this window, prolonged hydrothermal treatment may induce cycles of redissolution and recrystallisation [27, 57, 58]. Such processes can lead to a progressive reduction in average particle size, with a consequent increase in the SSA (Table 4). This makes the finer fraction of the product more susceptible to loss during the washing procedures, consistent with the experimental observation (Table 4).

Microwave heating was employed not only to reduce reaction times but also to minimise thermal gradients within the reaction vessel [31]. This feature is particularly advantageous for nanocube synthesis, as the higher reaction temperatures involved generate more severe thermal inhomogeneities compared to the 100 °C employed for the nanorod synthesis protocol. Unlike conventional hydrothermal synthesis where the autoclave walls are in thermal equilibrium with the fluid, microwave irradiation heats the solvent volumetrically while the Teflon liner remains relatively cooler. It has been proposed that this may create a 'cold wall' effect in the headspace that acts as an internal condenser, promoting continuous solvent evaporation and convection currents, although direct experimental verification of this effect was not performed in the present study. A reaction time of 4 h was selected as the baseline. Thanks to the lower polydispersity characterising the microwave-synthesised products (Table 5), the influence of the filling ratio could be delineated with greater clarity. Figure 7a,b compares two microwave-assisted syntheses performed with filling ratios of 23% and 46%, respectively. While the higher filling ratio (NC_MW_46%_E4) yielded nanocubes comparable in size and quality to the analogous conventional synthesis (NC_C_46%_E4_4 h), halving the filling ratio to 23% (NC_MW_23%_E4) significantly improved crystallinity. The product exhibited a more defined cubic morphology, with an average size that increased from 14 ± 4 nm to 26 ± 3 nm (Table 5).

As shown in detail in Table S7, the solvent composition changes dynamically with the filling ratio due to the differential evaporation rates of water and ethanol. At a reaction temperature of 200 °C, the final pressure in the sealed reactor reached approximately 19 bar (for details about the Python script used for the calculations, and the assumptions behind them, see the SI). A lower filling ratio corresponds to a larger headspace volume, which in turn promotes higher total solvent evaporation. This leads to a net increase in precursor concentration (Table S7), and a concomitant shift in the solvent composition, directly affecting the supersaturation ratio. This trend is consistent with the comparison between NC_MW_23%_E4 and NC_MW_46%_E4: the greater evaporation-driven volume reduction at lower filling ratios is expected to result in a higher effective concentration of precursor, promoting a higher growth rate throughout the reaction. Conversely, at higher filling ratios (46%), the lower effective concentration is expected to limit the growth rate, producing smaller and less well-defined nanocubes. To decouple these variables and isolate the effect of precursor concentration, a control series was conducted using pure water at filling ratios of 11%, 23% and 46%. TEM analysis (Figure 7c–e, respectively) confirms a general loss of well-defined cube-like nanoparticles in the absence of ethanol, particularly in NC_MW_46% (Figure 7e). Nevertheless, the inverse relationship between the filling ratio and the average nanoparticle size persists as the filling ratio increases (Table 5), consistent with the view that the evaporation-driven concentration gradient (Table S8) remains a primary determinant of growth kinetics. At lower filling ratios, where the concentration increase is maximal, a small fraction of cube-like particles can still be observed, suggesting that a threshold supersaturation level is required to favour anisotropic growth. The presence of ethanol in the original mixture may facilitate reaching this threshold by lowering the dielectric constant of the medium, thereby enhancing the supersaturation ratio compared to pure water. These results suggest a synergistic mechanism: while acetate ions appear necessary to promote the anisotropic cubic habit [45], a sufficiently high precursor concentration is also critical to provide the thermodynamic driving force necessary for full morphological definition.

TABLE 5 | Dimensional analysis of the nanocubes synthesised in the microwave oven. Crystallite sizes calculated using the Scherrer equation for the (111), (200), (220) and (311) reflections.

Sample name	NC_MW_11%	NC_MW_23%	NC_MW_46%	NC_MW_23%_E4	NC_MW_46%_E4
Size, nm	20 ± 3	25 ± 5	6 ± 1	26 ± 2	14 ± 3
SSA, m^2/g	46	73	81	45	47
Average crystallite size, nm	—	—	—	21.9 ± 0.5	14.4 ± 0.4

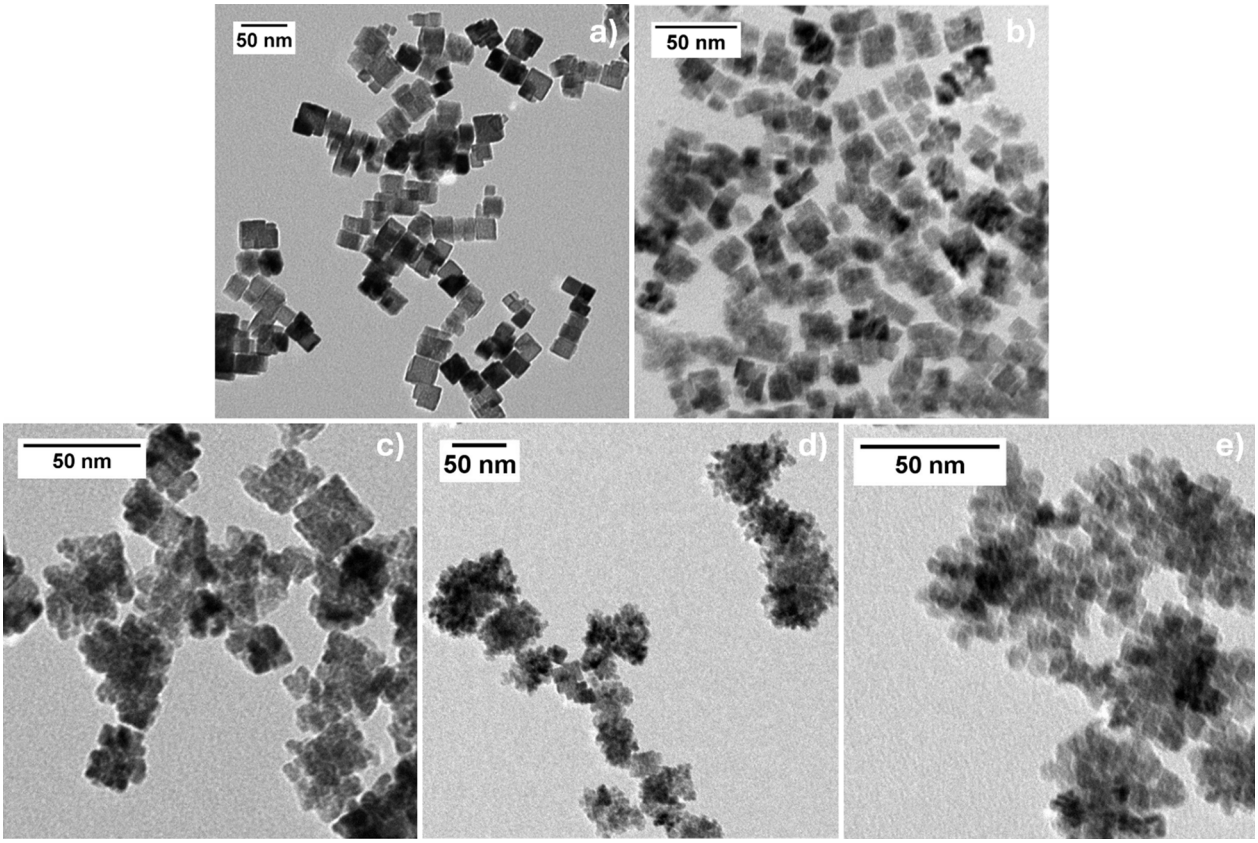

FIGURE 7 | Nanocubes obtained by microwave-assisted synthesis. Filling ratios of 23% (a) and 46% (b) and a 4 h reaction time. Products achieved without ethanol in solution and with filling ratios of 11% (c), 23% (d) and 46% (e).

SSAs of 45–47 $m^2 g^{-1}$ were achieved after just 4 h of reaction using both microwave and conventional heating (Tables 4 and 5). However, the microwave method yielded a better cube-like faceted morphology compared to the conventional analogue (comparing Figures 6a and 7a,b), effectively matching the quality obtained only after 24 h in the conventional process (sample NC_C_46%_E4_24 h). In other words, microwave-assisted synthesis, characterised by rapid and efficient volumetric heating with minimal thermal gradients, enabled the faster formation of well-defined nanoparticles with SSAs comparable to those produced via prolonged conventional heating. With just 4 h of microwave irradiation, the particle dimensions matched those obtained after 12–18 h of conventional treatment, yet the SSA remained considerably higher (Tables 4 and 5). In contrast, the significantly increased SSA observed for the ethanol-free samples (NC_MW_11%, NC_MW_23% and NC_MW_46%) can be attributed to the predominance of small, non-cubic nanoparticles approximately 8 nm in size (Figure 7c–e). TEM analysis revealed that while the sample synthesised at the highest filling ratio (46%) lacked defined features, a small fraction of cube-like nanoparticles could be discerned at lower filling ratios (11% and 23%), consistent with the evaporation-induced concentration increase. However, as previously discussed, the general absence of ethanol prevents the solubility drop required to drive the widespread formation of larger, faceted nanocubes, resulting overall in smaller crystallites with higher surface-to-volume ratios. Finally, the crystallite sizes estimated using the Scherrer equation (Tables 4 and 5) are in good agreement with the nanocube edge lengths measured via TEM, which is consistent with the hypothesis that the synthesised particles may consist of single crystals, although confirmation by high-resolution TEM (HRTEM) or selected area electron diffraction (SAED) would be required for definitive evidence.

4 | Conclusions

This study provides a comprehensive assessment of how reaction parameters, specifically precursor counter-ions, the filling ratio and solvent composition, govern the hydrothermal synthesis of ceria nanostructures. Regarding the nanorods, the choice of counter-ion proved to be the primary structure-directing factor. Chloride ions were essential for stabilising the anisotropic growth of rods by selectively adsorbing on the lateral facets, thereby suppressing radial growth and promoting longitudinal elongation. In contrast, nitrate ions promoted more isotropic growth towards the cubic morphology, while acetate ions resulted in the coexistence of both nanorods and nanocubes after 24 h. This suggests a competitive growth mechanism in which acetate ions effectively stabilise the (100) facets, diverting a fraction of the nuclei towards a cubic habit and thus partially inhibiting the longitudinal growth typical of the strongly alkaline environment. Notably, the microwave-assisted approach enabled a drastic reduction in reaction time, yielding crystalline nanorods in as little as 10 min. Crucially, unlike conventional heating, where prolonged times led to surface area loss due to coarsening, microwave synthesis preserved a high SSA while ensuring high

crystallinity. A synthetic route for nanocubes was also established using an acetate buffer solution. Here, the reactor filling ratio emerged as a decisive parameter for controlling nanocube size and morphology. Decreasing the filling ratio from 46% to 23% resulted in a marked increase in nanocube size, from 14 ± 4 nm to 26 ± 3 nm, and improved morphological definition. This behaviour is rationalised by considering the interplay between the reactor headspace and the solvent phase equilibrium. At lower filling ratios, the preferential evaporation of ethanol is proposed to lead to a higher precursor concentration and a lower dielectric environment, thereby enhancing the supersaturation ratio and driving a kinetic growth regime. Furthermore, the associated increase in precursor concentration proved critical for sharpening the particle facets. Experiments conducted in the absence of ethanol confirmed that while acetate ions appear necessary to dictate the cubic habit, a synergistic control of solvent composition and concentration is required to achieve well-defined morphologies. Taken together, these results establish a rational framework for the synthesis of ceria with defined morphology. By carefully modulating the reactor headspace and solvent composition, we demonstrated that microwave heating can be transformed from a simple, rapid heating tool into a versatile instrument for tuning physicochemical properties, laying the foundation for the production of advanced nanomaterials for catalytic and environmental applications [59, 60].

Author Contributions

Omar Bettini: conceptualisation, investigation, data curation, writing – original draft, visualisation. **Nicola Da Roit:** conceptualisation, data curation, writing – review and editing. **Andrea De Giacinto:** investigation, data curation, writing – review and editing. **Giulia Bragaggia:** writing – review and editing. **Paolo Dolcet**: software, writing – review and editing. **Jan-Dierk Grunwaldt:** writing – review and editing, funding acquisition. **Silke Behrens:** conceptualisation, writing – review and editing. **Silvia Gross:** conceptualisation, writing – review and editing, funding acquisition.

Acknowledgments

The authors thank the CRC 1441 'Track Act' (Project-ID 426888090) for financial support to this project. S.G. gratefully acknowledges DFG for the funding of a Mercator Fellowship position in the terms 2020–2024 and 2025–2028 within the CRC 1441 'Track Act'.

Open access publishing facilitated by Universita degli Studi di Padova, as part of the Wiley – CRUI-CARE agreement.

Funding

This study was supported by the Deutsche Forschungsgemeinschaft (DFG, German Research Foundation)-CRC 1441 (Project-ID 426888090).

Conflicts of Interest

The authors declare no conflicts of interest.

Data Availability Statement

The data that supports the findings of this study are available in the Supporting Information of this article.

Declaration of Generative AI and AI-Assisted Technologies in the Writing Process

During the preparation of this work the authors used Gemini 3 Flash to improve the quality and clarity of English language of some manuscript parts. Claude 4.5 Sonnet has been used for the preparation of the Python script used to calculate the pressure inside of the hydrothermal reactors (cf. Ref. [60]). After using these tools, the authors reviewed and edited the content as needed and take full responsibility for the content of the published article.

References

1. R. M. Al Soubaihi, K. M. Saoud, and J. Dutta, "Critical Review of Low-Temperature CO Oxidation and Hysteresis Phenomenon on Heterogeneous Catalysts," *Catalysts* 8, no. 12 (2018): 660, https://doi.org/10.3390/catal8120660.

2. F. Maurer, A. Beck, J. Jelic, et al., "Surface Noble Metal Concentration on Ceria as a Key Descriptor for Efficient Catalytic CO Oxidation," *ACS Catalysis* 12, no. 4 (2022): 2473–2486, https://doi.org/10.1021/acscatal.1c04565.

3. D. Gashnikova, F. Maurer, E. Sauter, et al., "Highly Active Oxidation Catalysts through Confining Pd Clusters on CeO_2 Nano-Islands," *Angewandte Chemie International Edition* 63, no. 35 (2024): e202408511, https://doi.org/10.1002/anie.202408511.

4. B. S. V. Gosen, P. L. Verplanck, K. R. Long, J. Gambogi, and R. R. Seal, Rare-Earth Elements, 2017, https://doi.org/10.3133/PP1802O, Professional Paper.

5. D. R. Mullins, "The Surface Chemistry of Cerium Oxide," *Surface Science Reports* 70 (2015): 42–85, https://doi.org/10.1016/j.surfrep.2014.12.001.

6. A. Trovarelli and J. Llorca, "Ceria Catalysts at Nanoscale: How Do Crystal Shapes Shape Catalysis?," *ACS Catalysis* 7, no. 7 (2017): 4716–4735, https://doi.org/10.1021/acscatal.7b01246.

7. X. Liu, K. Zhou, L. Wang, B. Wang, and Y. Li, "Oxygen Vacancy Clusters Promoting Reducibility and Activity of Ceria Nanorods," *Journal of the American Chemical Society* 131, no. 9 (2009): 3140–3141, https://doi.org/10.1021/ja808433d.

8. P. Li, X. Chen, Y. Li, and J. W. Schwank, "A Review on Oxygen Storage Capacity of CeO2-Based Materials: Influence Factors, Measurement Techniques, and Applications in Reactions Related to Catalytic Automotive Emissions Control," *Catalysis Today* 327 (2019): 90–115, https://doi.org/10.1016/j.cattod.2018.05.059.

9. A. Trovarelli and P. Fornasiero, *Catalysis by Ceria and Related Materials*, (Imperial College Press, 2002).

10. S. Datta and L. Torrente-Murciano, "Nanostructured Faceted Ceria as Oxidation Catalyst," *Current Opinion in Chemical Engineering* 20 (2018): 99–106, https://doi.org/10.1016/j.coche.2018.03.009.

11. D. Mukherjee and B. M. Reddy, "Significance of Oxygen Storage Capacity of Catalytic Materials in Emission Control Application," *Emission Control Science and Technology* 6, no. 4 (2020): 381–389, https://doi.org/10.1007/S40825-020-00170-2.

12. T. X. T. Sayle, S. C. Parker, and C. R. A. Catlow, "Surface Oxygen Vacancy Formation on CeO_2 and Its Role in the Oxidation of Carbon Monoxide," *Journal of the Chemical Society, Chemical Communications* 28, no. 14 (1992): 977–978, https://doi.org/10.1039/C39920000977.

13. M. Nolan, S. C. Parker, and G. W. Watson, "The Electronic Structure of Oxygen Vacancy Defects at the Low Index Surfaces of Ceria," *Surface Science* 595, no. 1 (2005): 223–232, https://doi.org/10.1016/J.SUSC.2005.08.015.

14. A. M. Gänzler, M. Casapu, D. E. Doronkin, et al., "Unravelling the Different Reaction Pathways for Low Temperature CO Oxidation on Pt/CeO_2 and Pt/Al_2O_3 by Spatially Resolved Structure-Activity Correlations," *Journal of Physical Chemistry Letters* 10, no. 24 (2019): 7698–7705, https://doi.org/10.1021/acs.jpclett.9b02768.

15. M. Cargnello, V. V. T. Doan-Nguyen, T. R. Gordon, et al., "Control of Metal Nanocrystal Size Reveals Metal-Support Interface Role for Ceria Catalysts," *Science* 341, no. 6147 (2013): 771–773, https://doi.org/10.1126/science.1240148.

16. Z. Wu and S. H. Overbury, *Catalysis by Materials with Well-Defined Structures*, (Elsevier Inc, 2015), https://doi.org/10.1016/C2013-0-14362-0.

17. M. Nolan, J. E. Fearon, and G. W. Watson, "Oxygen Vacancy Formation and Migration in Ceria," *Solid State Ionics* 177, no. 35 (2006): 3069–3074, https://doi.org/10.1016/j.ssi.2006.07.045.

18. S. Yang and L. Gao, "Controlled Synthesis and Self-Assembly of CeO_2 Nanocubes," *Journal of the American Chemical Society* 128, no. 29 (2006): 9330–9331, https://doi.org/10.1021/ja063359h.

19. Z. Hu, X. Liu, D. Meng, Y. Guo, Y. Guo, and G. Lu, "Effect of Ceria Crystal Plane on the Physicochemical and Catalytic Properties of Pd/Ceria for CO and Propane Oxidation," *ACS Catalysis* 6, no. 4 (2016): 2265–2279, https://doi.org/10.1021/acscatal.5b02617.

20. I. Florea, C. Feral-Martin, J. Majimel, D. Ihiawakrim, C. Hirlimann, and O. Ersen, "Three-Dimensional Tomographic Analyses of CeO_2 Nanoparticles," *Crystal Growth & Design* 13, no. 3 (2013): 1110–1121, https://doi.org/10.1021/cg301445h.

21. L. Yan, R. Yu, J. Chen, and X. Xing, "Template-Free Hydrothermal Synthesis of CeO_2 Nano-octahedrons and Nanorods: Investigation of the Morphology Evolution," *Crystal Growth & Design* 8, no. 5 (2008): 1474–1477, https://doi.org/10.1021/cg800117v.

22. Z. Ji, X. Wang, H. Zhang, et al., "Designed Synthesis of CeO_2 Nanorods and Nanowires for Studying Toxicological Effects of High Aspect Ratio Nanomaterials," *ACS Nano* 6, no. 6 (2012): 5366–5380, https://doi.org/10.1021/nn3012114.

23. G. Spezzati, A. D. Benavidez, A. T. DeLaRiva, et al., "CO Oxidation by Pd Supported on CeO_2(100) and CeO_2(111) Facets," *Applied Catalysis B: Environmental* 243 (2019): 36–46, https://doi.org/10.1016/j.apcatb.2018.10.015.

24. C. Yang, X. Yu, S. Heißler, et al., "Surface Faceting and Reconstruction of Ceria Nanoparticles," *Angewandte Chemie International Edition* 56, no. 1 (2017): 375–379, https://doi.org/10.1002/anie.201609179.

25. C. Yang, X. Ning, S. Chen, et al., "Fine Control for the Preparation of Ceria Nanorods (111)," *RSC Advances* 13, no. 31 (2023): 21271–21276, https://doi.org/10.1039/D3RA02817H.

26. F. Barbon, F. Tajoli, F. Spolaore, and S. Gross, "Further Sustainable and/or Unconventional Low-Temperature Wet-Chemical Synthetic Methods," in *Unconventional Green Synthesis of Inorganic Nanomaterials*, ed. S. Gross, (Royal Society of Chemistry, 2024), 315–429, https://doi.org/10.1039/9781839165757-00315.

27. R. I. Walton, "Perovskite Oxides Prepared by Hydrothermal and Solvothermal Synthesis: A Review of Crystallisation, Chemistry, and Compositions," *Chemistry – A European Journal* 26, no. 42 (2020): 9041–9069, https://doi.org/10.1002/chem.202000707.

28. B. S. Wee, S. A. E. Halim, and T. F. Choo, "Simple Hydrothermal Synthesis of Ultra-Small Cerium Oxide Nanoparticles," *Journal of Cluster Science* 35, no. 6 (2024): 2061–2068, https://doi.org/10.1007/s10876-024-02644-7.

29. S. Feng and R. Xu, "New Materials in Hydrothermal Synthesis," *Accounts of Chemical Research* 34, no. 3 (2001): 239–247, https://doi.org/10.1021/ar0000105.

30. A. Rabenau, "The Role of Hydrothermal Synthesis in Preparative Chemistry," *Angewandte Chemie International Edition in English* 24, no. 12 (1985): 1026–1040, https://doi.org/10.1002/ANIE.198510261.

31. F.-F. Chen and Y.-J. Zhu, "Highly Efficient Rapid Preparation of Inorganic Nanostructured Materials by Microwave Heating," in *Unconventional Green Synthesis of Inorganic Nanomaterials*, ed. S. Gross, (Royal Society of Chemistry, 2024), 141–251, https://doi.org/10.1039/9781839165757-00141.

32. H. Moreno, L. S. R. Rocha, G. Garcia, et al., "Tuning Ceria-Based Nanomaterials: The Effects of Chemical Potential and Mineralizing Agents on Atmosphere-Induced Electrical Resistance," *Materials Research Bulletin* 197 (2026): 113987, https://doi.org/10.1016/j.materresbull.2025.113987.

33. G. Yang and S.-J. Park, "Conventional and Microwave Hydrothermal Synthesis and Application of Functional Materials: A Review," *Materials* 12, no. 7 (2019): 1177, https://doi.org/10.3390/ma12071177.

34. K. Ocakoglu, Sh A. Mansour, S. Yildirimcan, A. A. Al-Ghamdi, F. El-Tantawy, and F. Yakuphanoglu, "Microwave-Assisted Hydrothermal Synthesis and Characterization of ZnO Nanorods," *Spectrochimica Acta Part A: Molecular and Biomolecular Spectroscopy* 148 (2015): 362–368, https://doi.org/10.1016/j.saa.2015.03.106.

35. Y. Hu, C. Liu, Y. Zhang, N. Ren, and Y. Tang, "Microwave-Assisted Hydrothermal Synthesis of Nanozeolites with Controllable Size," *Microporous and Mesoporous Materials* 119, no. 1 (2009): 306–314, https://doi.org/10.1016/j.micromeso.2008.11.005.

36. J. D. C. Carregosa, J. P. F. Grilo, G. S. Godoi, D. A. Macedo, R. M. Nascimento, and R. M. P. B. Oliveira, "Microwave-Assisted Hydrothermal Synthesis of Ceria (CeO_2): Microstructure, Sinterability and Electrical Properties," *Ceramics International* 46, no. 14 (2020): 23271–23275, https://doi.org/10.1016/j.ceramint.2020.06.021.

37. L.-Y. Meng, B. Wang, M.-G. Ma, and K.-L. Lin, "The Progress of Microwave-Assisted Hydrothermal Method in the Synthesis of Functional Nanomaterials," *Materials Today Chemistry* 1 (2016): 63–83, https://doi.org/10.1016/j.mtchem.2016.11.003.

38. T. W. Wong, "Electrical, Magnetic, Photomechanical and Cavitational Waves to Overcome Skin Barrier for Transdermal Drug Delivery," *Journal of Controlled Release* 193 (2014): 257–269, https://doi.org/10.1016/j.jconrel.2014.04.045.

39. A. I. Y. Tok, F. Y. C. Boey, Z. Dong, and X. L. Sun, "Hydrothermal Synthesis of CeO_2 Nano-Particles," *Journal of Materials Processing Technology* 190, no. 1 (2007): 217–222, https://doi.org/10.1016/j.jmatprotec.2007.02.042.

40. A. I. Y. Tok, S. W. Du, F. Y. C. Boey, and W. K. Chong, "Hydrothermal Synthesis and Characterization of Rare Earth Doped Ceria Nanoparticles," *Materials Science and Engineering: A* 466, no. 1 (2007): 223–229, https://doi.org/10.1016/j.msea.2007.02.083.

41. A. Annamalai, Y. D. Eo, C. Im, and M.-J. Lee, "Surface Properties and Dye Loading Behavior of Zn_2SnO_4 Nanoparticles Hydrothermally Synthesized Using Different Mineralizers," *Materials Characterization* 62, no. 10 (2011): 1007–1015, https://doi.org/10.1016/j.matchar.2011.07.006.

42. K. Edalati, A. Shakiba, J. Vahdati-Khaki, and S. M. Zebarjad, "Low-Temperature Hydrothermal Synthesis of ZnO Nanorods: Effects of Zinc Salt Concentration, Various Solvents and Alkaline Mineralizers," *Materials Research Bulletin* 74 (2016): 374–379, https://doi.org/10.1016/j.materresbull.2015.11.001.

43. Q. Wu, F. Zhang, P. Xiao, et al., "Great Influence of Anions for Controllable Synthesis of CeO_2 Nanostructures: From Nanorods to Nanocubes," *Journal of Physical Chemistry C* 112, no. 44 (2008): 17076–17080, https://doi.org/10.1021/jp804140e.

44. Y. Xu, P. Koshy, S. S. Mofarah, and C. C. Sorrell, "Morphological Mapping of Hydrothermally Synthesised Nanoceria at High Ce Concentrations," *ChemNanoMat* 8, no. 9 (2022): e202200132, https://doi.org/10.1002/cnma.202200132.

45. Y. Fu, C. J. Neal, E. Kolanthai, et al., "Effect of Acetate Ions and pH on the Morphology of Cerium Oxide Nanoparticles," *Colloids and Surfaces A: Physicochemical and Engineering Aspects* 679 (2023): 132616, https://doi.org/10.1016/j.colsurfa.2023.132616.

46. G.-M. Lyu, Y.-J. Wang, X. Huang, et al., "Hydrophilic CeO_2 Nanocubes Protect Pancreatic β-Cell Line INS-1 from H_2O_2-Induced Oxidative Stress," *Nanoscale* 8, no. 15 (2016): 7923–7932, https://doi.org/10.1039/C6NR00826G.

47. S. Brunauer, P. H. Emmett, and E. Teller, "Adsorption of Gases in Multimolecular Layers," *Journal of the American Chemical Society* 60, no. 2 (1938): 309–319, https://doi.org/10.1021/ja01269a023.

48. H.-X. Mai, L.-D. Sun, Y.-W. Zhang, et al., "Shape-Selective Synthesis and Oxygen Storage Behavior of Ceria Nanopolyhedra, Nanorods, and Nanocubes," *Journal of Physical Chemistry B* 109, no. 51 (2005): 24380–24385, https://doi.org/10.1021/jp055584b.

49. H. S. Wasly, M. S. A. El-Sadek, and M. Henini, "Influence of Reaction Time and Synthesis Temperature on the Physical Properties of ZnO Nanoparticles Synthesized by the Hydrothermal Method," *Applied Physics A* 124, no. 1 (2018): 76, https://doi.org/10.1007/s00339-017-1482-4.

50. T. V. Khai, L. N. Long, N. H. T. Khoi, and N. Hoc Thang, "Effects of Hydrothermal Reaction Time on the Structure and Optical Properties of ZnO/Graphene Oxide Nanocomposites," *Crystals* 12, no. 12 (2022): 1825, https://doi.org/10.3390/cryst12121825.

51. O. Bettini, S. Battiston, N. Da Roit, et al., Submitted to Green Chemistry.

52. L. Torrente-Murciano, A. Gilbank, B. Puertolas, T. Garcia, B. Solsona, and D. Chadwick, "Shape-Dependency Activity of Nanostructured CeO_2 in the Total Oxidation of Polycyclic Aromatic Hydrocarbons," *Applied Catalysis B: Environmental* 132 (2013): 116–122, https://doi.org/10.1016/j.apcatb.2012.10.030.

53. R. I. Walton, "Solvothermal Synthesis of Cerium Oxides," *Progress in Crystal Growth and Characterization of Materials* 57, no. 4 (2011): 93–108, https://doi.org/10.1016/j.pcrysgrow.2011.10.002.

54. N. Singhania, E. A. Anumol, N. Ravishankar, and G. Madras, "Influence of CeO_2 Morphology on the Catalytic Activity of CeO_2 –Pt Hybrids for CO Oxidation," *Dalton Transactions* 42, no. 43 (2013): 15343–15354, https://doi.org/10.1039/C3DT51364E.

55. O. Altıntaş, M. Aksoy, E. Ünal, M. Karaaslan, and C. Sabah, "Operating Frequency Reconfiguration Study for a Split Ring Resonator Based Microfluidic Sensor," *Journal of the Electrochemical Society* 167, no. 14 (2020): 147512, https://doi.org/10.1149/1945-7111/abc656.

56. M. Mohsen-Nia, H. Amiri, and B. Jazi, "Dielectric Constants of Water, Methanol, Ethanol, Butanol and Acetone: Measurement and Computational Study," *Journal of Solution Chemistry* 39, no. 5 (2010): 701–708, https://doi.org/10.1007/s10953-010-9538-5.

57. J. W. Annis, J. M. Fisher, D. Thompsett, and R. I. Walton, "Solvothermal Synthesis Routes to Substituted Cerium Dioxide Materials," *Inorganics* 9, no. 6 (2021): 40, https://doi.org/10.3390/inorganics9060040.

58. R. I. Walton, *Solvothermal and Hydrothermal Methods for Preparative Solid-State Chemistry*, (Elsevier, 2023), 40–110, https://doi.org/10.1016/B978-0-12-823144-9.00068-6.

59. I. H. Bell, J. Wronski, S. Quoilin, and V. Lemort, "Pure and Pseudo-Pure Fluid Thermophysical Property Evaluation and the Open-Source Thermophysical Property Library CoolProp," *Industrial & Engineering Chemistry Research* 53, no. 6 (2014): 2498–2508, https://doi.org/10.1021/ie4033999.

60. P. Dolcet, Calculator for Pressure and Viscosity Within Closed Vessels, for Pure and Binary Mixture of Fluids, 2026, https://doi.org/10.5281/zenodo.21218425.

Supporting Information

Additional supporting information can be found online in the Supporting Information section. The Supporting Information is available online and includes further TEM images, histograms with dimensional distribution and a description of the Python script used to calculate the pressure within the hydrothermal reactors and additional discussion [59, 60].